SMASIS2017-3754

Harnessing the Quasi-Zero Stiffness from Fluidic Origami for Low Frequency Vibration Isolation

Sahand Sadeghi

Department of Mechanical Engineering Clemson University Clemson, SC, USA

Suyi Li*

Department of Mechanical Engineering Clemson University Clemson, SC, USA

ABSTRACT

This research investigates a quasi-zero stiffness (QZS) property from the pressurized fluidic origami cellular solid, and examines how this QZS property can be harnessed for lowfrequency base excitation isolation. The QZS property originates from the nonlinear geometric relations between folding and internal volume change, and it is directly correlated to the design parameters of the constituent Miura-Ori sheets. Two different structures are studied to obtain a design guideline for achieving QZS: one is identical stacked Miura-Ori sheets (ismo) and the other is non-identical stacked Miura-Ori sheets (nismo). Further dynamic analyses based on numerical simulation and harmonic balance method, indicate that the QZS from pressurized fluidic origami can achieve effective base excitation isolation at low frequencies. Results of this study can become the foundation of origami-inspired metamaterials and metastructures with embedded dynamic functionalities.

1. INTRODUCTION

Origami – the ancient Japanese paper folding art [1] – is being transformed into a framework of design and fabrication tools for a wide variety of engineering systems. The kinematics of folding flat sheets into sophisticated 3D shapes offers many desirable characteristics for creating deployable aerospace structures [2], kinetic architectures [3,4], self-folding robots [5], compact surgery devices [6,7], crash box impact absorbers [8], and many others [9–11]. Recently, there is a paradigm shift from harnessing the kinematics of origami to exploiting the energetics or mechanics of folding. As a result, a new category of origami-based mechanical metamaterials emerged [12]. In particular, one can stack and connect multiple origami sheets together to

Despite the significant progress in the mechanics studies of origami structures and materials, the vast majority of the aforementioned previous works are centered on static responses. The investigation on the dynamics of origami folding is still a nascent field. Yasuda et al. investigated the nonlinear wave propagation in multiple-degree-of freedom origami solid [27]; Ishida examined the feasibility of using bistable Kresling origami for vibration isolation [28], and Fang et al. studied the dynamic characteristics of a bistable origami structure [29]. Other than these studies, there are no other literatures on this interesting and important subject. Therefore, this research aims at expanding our knowledge on how to harness the foldinginduced mechanical properties for dynamic applications. Specifically, the research examines a unique quasi-zero-stiffness (QZS) from the pressurized fluidic origami, and investigates how this QZS property can be used for low-frequency vibration isolation.

create an architectured material, and exploit the intricate relationships between folding and constituent sheet deformations to achieve unique material properties. For example, negative and flipping Poisson's ratio can be achieved from the folding-induced coupling among in-plane and out-of-plane strains [13–17]. Self-locking and discrete stiffness-jump are possible via the facet binding behaviors from non-flat foldable creases [18,19]. Elastic multi-stability is also feasible due to the nonlinear correlations among crease and facet deformations during folding [20–23]. Furthermore, the stacked origami architecture consists of naturally embedded tubes that can be pressurized to create adaptive functions. Such pressurized stacked-origami concept is also called fluidic origami, and it has been shown that it can exhibit shape transformation, stiffness control, and recoverable collapse [24–26].

^{*} Corresponding author: suyil@clemson.edu

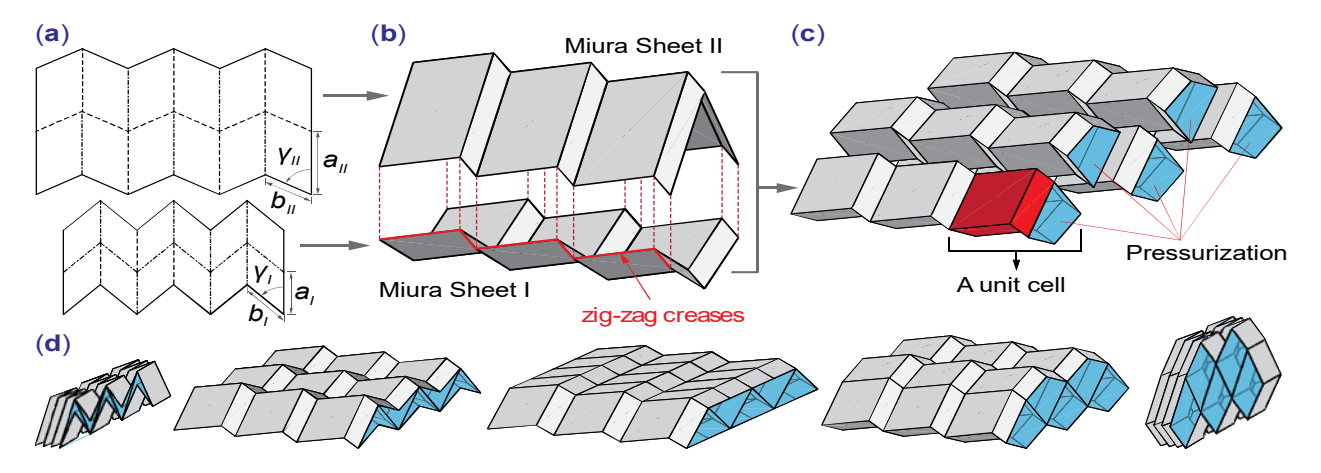


Figure 1. The concept of fluidic origami. (a) Miura-Ori sheets are defined by three design parameters. (b) Stacking two compatible Miura-Ori sheets along their zig-zag creases can form a tubular structure. (c) Integration of different pressurized origami tubes into a 3D configuration. (d) As the fluidic origami folds, its enclosed volumes change accordingly, which is essential for achieving the guasi-zero stiffness (figure adopted from [24]).

The research presented in this paper can be divided into two parts. The first part investigates the physical origin of the quasizero stiffness and its correlation to the fluidic origami design. Two cases are discussed: identical stacked Miura-Ori sheets (ismo) and non-identical stacked Miura-Ori sheets (nismo). It is shown that the QZS property arises due to the nonlinear geometric relationships between folding and internal volume change, and the reaction force corresponding to the QZS configuration can be tailored via pressure control. This research also discusses the origami design criteria to achieve QZS.

The second part of this research examines how such OZS property could be harnessed for adaptive and low-frequency vibration isolation. Low-frequency vibration isolation has been the concern of mechanical and civil engineers for many years. For a mass (m) supported by a linear spring of stiffness (k), it has been shown that vibration isolation occurs in frequencies over $\sqrt{2k/m}$ [30]. Therefore, to gain a wider usable frequency bandwidth for vibration isolation, it is desirable to have a smaller stiffness k; however, this would result in a large static displacement. An effective solution to this problem is to incorporate nonlinear springs with QZS characteristics. For example, with proper spatial arrangements and stiffness assignments, it is possible to combine linear springs to create a QZS isolator with zero dynamic stiffness [31–33]. Via both analytical solutions and numerical simulations, this research shows that the QZS properties of pressurized fluidic origami can effectively isolate base excitations at low frequencies. Therefore, results for this research can open up new avenues towards origami-based metamaterials and structures with programmable dynamic applications.

The rest of this paper will be organized as follows. Section 2 focuses on the nonlinear geometrical relationships between origami folding and QZS characteristics. Section 3 discusses the dynamic analysis of utilizing the investigated QZS property for base excitation isolation. Approximate solutions based on the harmonic balance method are presented and compared to

numerical simulations. Finally, section 4 concludes this paper with summary and discussions.

2. Geometry of Folding and the Physical Principle of Achieving QZS

A set of kinematically compatible tubular cells, made by stacking two Miura-Ori folded sheets along their zig-zag crease lines, are the building blocks of fluidic origami (Figures 1) [24,25]. Miura-Ori is a periodic tessellation, thus it is possible to study the unit cell shown in Figure 2 as a representative of the whole structure. The governing geometrical relations of Miura-Ori have been studied before and they are briefly reviewed here. The design of Miura-Ori can be described by three parameters that remain constants regardless of folding. They are the length of two adjacent crease lines (a and b), and the angle between these two lines (γ) (Figure 1a).

Miura-Ori is rigid foldable, thus one can assume that the facet material is rigid and the crease lines behave like ideal hinges. Therefore, the folding motion of Miura-Ori has a one-degree-of-freedom and it can be described by the dihedral folding angle (θ) defined between the x-y reference plane and the constituent facets (Figure 2).

In order to satisfy the kinematical compatibility of the Miura-Ori and prevent any separation of the two sheets during folding, two conditions need to be satisfied [13]:

$$b_{II} = b_{I} = b, \tag{1}$$

$$a_I \cos \gamma_I = a_{II} \cos \gamma_{II}. \tag{2}$$

In addition, the folding angles of two Miura-Ori sheets are related by the following equation:

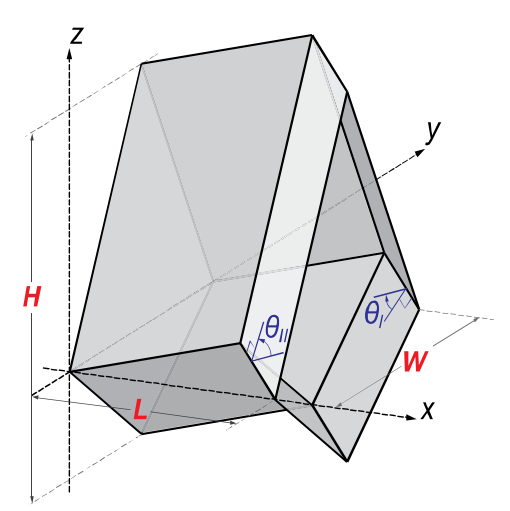


Figure 2. The geometry of the unit cell. θ_{l} and θ_{ll} are the dihedral folding angles of Miura-Ori sheet I and II, respectively (Figure adopted from [24])

$$\cos \theta_{II} \tan \gamma_{II} = \cos \theta_{I} \tan \gamma_{I} \tag{3}$$

As a result of these kinematic constraints, rigid folding of the fluidic origami is still a one degree of freedom mechanism, and the corresponding kinematic characteristics could be described based on one independent variable. In this paper we choose the folding angle θ_I for such a purpose. Therefore, the unit cell length, width and height can be calculated as follows, [24]:

$$L = \frac{2b\cos\theta_I \tan\gamma_I}{\sqrt{1 + \cos^2\theta_I \tan^2\gamma_I}},\tag{4}$$

$$W = 2a_I \sqrt{1 - \sin^2 \theta_I \sin^2 \gamma_I}, \tag{5}$$

$$H = a_{II} \sin \theta_{II} \sin \gamma_{II} - a_{I} \sin \theta_{I} \sin \gamma_{I}. \tag{6}$$

Based on these variables, the enclosed volume of a unit cell can be calculated as follows [24]:

$$V = 2a_I^2 b \sin^2 \gamma_I \cos \theta_I \left(\sqrt{\frac{\tan^2 \gamma_{II}}{\tan^2 \gamma_I} - \cos^2 \theta_I} + \sin \theta_I \right). \tag{7}$$

Equations (4-7) elucidate the kinematic connections between the external geometries and internal volume of fluidic origami. Based on these relationships, one can predict that the fluidic origami will fold to a configuration with maximum enclosed volume when it is subject to internal pressure [26]. This is due to the entropy increase from inner energy reduction by volume expansion [34]. Pressurization can also imparts nonlinear stiffness to the structure (pressure-induced stiffness) [26]. If the fluidic origami structure is subjected to external mechanical loads along the -x direction (defined in Figure 2), the reaction force due to internal pressure can be calculated as follows based on virtual work principle:

$$F_{L} = -P\frac{dV}{dL} = -P\frac{dV}{d\theta_{I}} \left(\frac{dL}{d\theta_{I}}\right)^{-1},\tag{8}$$

where dL is the change in origami length along the external force exertion direction. The corresponding pressure-induced stiffness is defined as the variation of the reaction force with respect to infinitesimal deformation [26]:

$$K_L = \frac{\partial F_L}{\partial L}. (9)$$

In order to investigate the feasibility of reaching QZS characteristics, we consider the following scenario in this research. The fluidic origami is pressurized at first based on an initial pressure (P_i) until it folds and settles at the configuration with maximum possible internal volume (V_i). Then the fluidic origami is sealed so that the total amount of pressurized gas inside is kept constant. After this, if the fluidic origami deforms via folding due to external forces, its internal pressure (P) and enclosed volume (V) will change accordingly. The ideal gas law states that:

$$PV = nRT, (10)$$

where n is the amount of substance of gas (in moles), R is the universal gas constant, and T is the absolute temperature of the gas. If the change in internal volume due to folding occurs slowly, the gas temperature can be assumed constant so that:

$$PV = P_i V_i = const, (11)$$

and the reaction force equation (8) can be updated as,

(7)
$$F_L = -\frac{P_i V_i}{V} \frac{dV}{d\theta_I} \left(\frac{dL}{d\theta_I}\right)^{-1}.$$
 (12)

Equation (8,9) and (12) reveal that the pressure-induced reaction force and stiffness is strongly nonlinear and they are dictated by the kinematics of folding. Therefore, with appropriate origami design, it is possible to achieve the desired quasi-zero stiffness for vibration isolation. In the following subsections, two different design cases are considered to illustrate how to harness the origami folding and internal pressure to achieve quasi-zero stiffness. The first case is Identical Stacked Miura-Ori sheets (ISMO) and the second one is Non-Identical Stacked Miura-Ori sheets (NISMO).

2.1 Case 1: Identical Stacked Miura-Ori sheets (ISMO)

If the two Miura-Ori sheets are identical, the geometric relationships discussed previously are simplified because $\gamma_{II} = \gamma_I = \gamma$ and $a_{II} = a_I = a$. Figure 3 shows the different reaction force-deformation curves of a ISMO cell assuming either 1) constant pressure, which was previously studied by the authors for recoverable collapse [26], or 2) constant PV. The initial pressure of both cases are the same at 13.8 kPa. The nonlinearity governed by folding is evident in these force-deformation curves. Especially, the curve with constant PV has a segment of negative stiffness (dashed line in Figure 3) between two segments with positive stiffness.

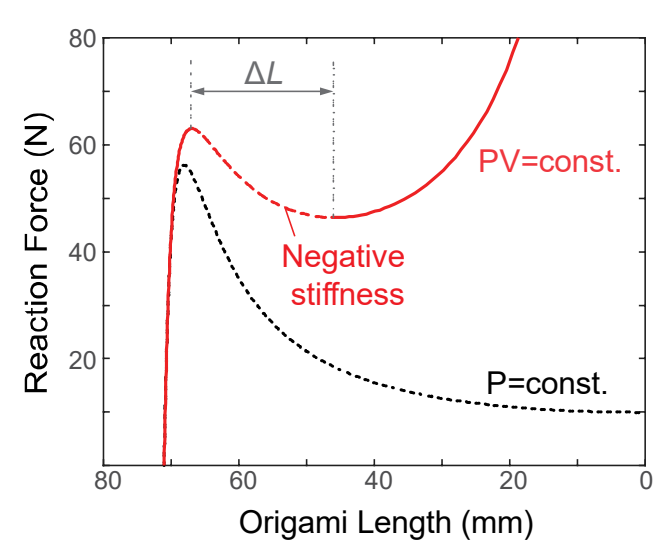


Figure 3. Reaction force-deformation curve of a fluidic origami with a=b=38mm, and $y=75^{\circ}$.

Results in Figure 3 also imply that it would be possible to achieve quasi-zero-stiffness by choosing proper design parameters for the origami when PV = const. Indeed, figure 4 shows the force-deformation curves of different ISMO cells based on the same crease lengths (a = b = 38 mm) but different γ angles. It can be seen that when the sector angle γ is less than 69°, the reaction force increases monotonically with

deformation, implying a nonlinear positive stiffness. When $\gamma > 69^\circ$, the reaction force curve has a segment of negative stiffness. The critical, quasi-zero-stiffness can be achieved when the sector angle equals to 69° . At this particular sector angle, the length of the negative stiffness segment in the reaction force curve converges to zero. In another word, the tangent stiffness of the fluidic origami is positive throughout its deformation range, except that at the QZS configuration the tangent stiffness equals to zero.

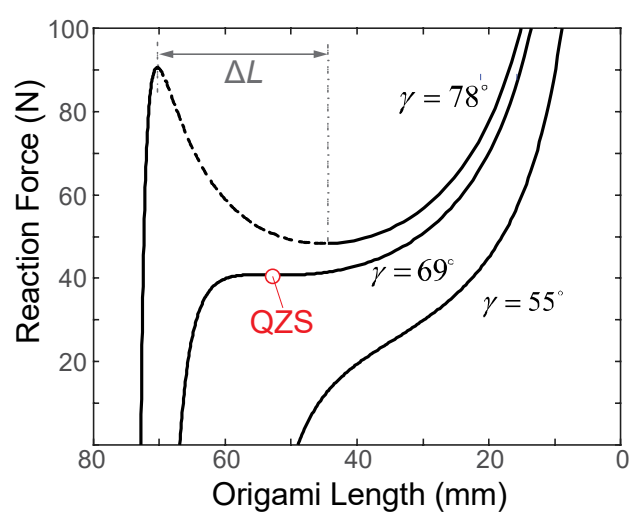


Figure 4. The influence of γ angle on the force-deformation relationship

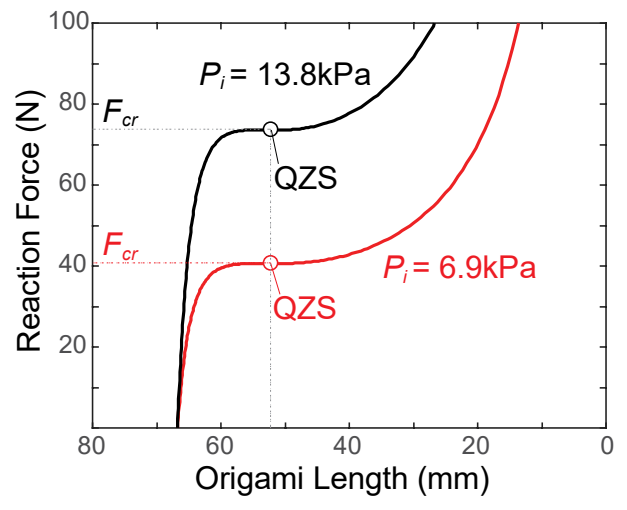


Figure 5. Reaction force-deformation curve of a fluidic origami with PV=const. based on different initial pressures (*Pi*).

There are several interesting properties from the ISMO fluidic origami with $\gamma = 69^{\circ}$. First of all, it can achieve the QZS

property regardless of the initial pressure (P_i) . Secondly, the magnitude of reaction force at the QZS point (F_{cr}) is linearly proportional to the magnitude of initial pressure. Finally, the deformation at the QZS point is only a function of origami geometry (Figure 5). Later in this paper, we will discuss how these properties can be beneficial for vibration isolation. In order to find a comprehensive design criteria to obtain QZS characteristics, a non-dimensional parameter w is introduced as follows:

$$w = \frac{\Delta l}{b} \tag{13}$$

where Δl is the deformation range with negative stiffness in the reaction force-deformation curves (Figure 3, 4), and b is the common crease length of the two Miura-Ori sheets (Figure 1). For reaching the QZS, it is desirable to have Δl equal to zero. The parametric study result in Figure 6 illustrates the correlation between w and the Miura-Ori design parameters. It can be concluded that when the two Miura-Ori sheets are identical, the magnitude of w is independent of k (= a/b) and only depends on the γ angle. That is, QZS is reachable only when $\gamma = 69^\circ$ regardless of the a and b crease lengths.

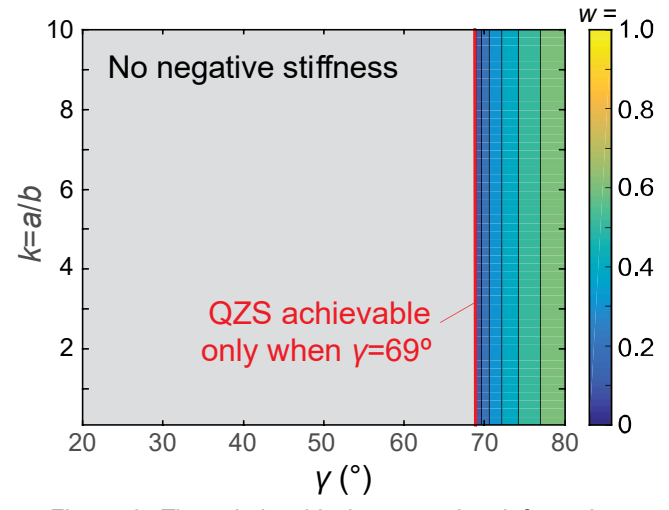


Figure 6. The relationship between the deformation range with negative stiffness and ISMO design parameters. Gray region represent designs that would not generate any negative stiffness.

2.2 CASE 2: NON-IDENTICAL STACKED MIURA-ORI SHEETS (NISMO)

To study the case that two Miura-Ori sheets are not identical, we introduce a non-dimensional parameter Γ as follows to

characterize the differences between the two Miura sheet designs:

$$\Gamma = \frac{a_{II}}{a_I}.\tag{14}$$

Following the similar approach as in the ISMO case, it is possible to analyze the design parameters and the feasibility of reaching QZS. Figure 7 illustrates the correlation between Miura-Ori design parameter and the non-dimensional parameter w. In the NISMO case, the designs that can provide QZS depend both on the sector angles and the crease line lengths. The parametric study results in Figure 6 and 7 can serve as design guidelines for the dynamic analyses discussed in the following section.

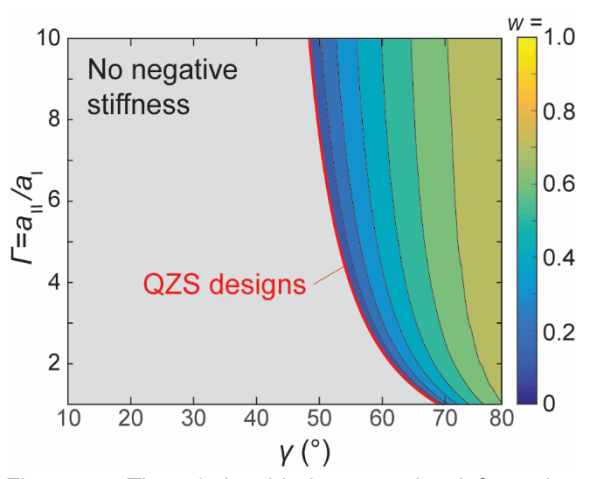


Figure 7. The relationship between the deformation range with negative stiffness and NISMO design parameters. Gray region represent designs that would not generate any negative stiffness.

3. Base Excitation Isolation via the QZS property of fluidic origami

After investigating the physical origins and design guidelines of the pressure induced QZS in fluidic origami, the following section of this paper turns to examine the effectiveness of harnessing the QZS for low-frequency base excitation isolation. Figure 8a illustrates the schematic of fluidic origami being used for vibration isolation, where the fluidic origami itself is assumed massless and a lumped mass (m) is attached at the top.

In this setup, the origami structure can be described as a combination of a nonlinear spring and damping between the base and lumped mass (Figure 8b). The governing dynamic equation of motion can be written as:

$$\ddot{u} + 2\zeta \dot{u} + F = \Omega^2 Y \cos \Omega t \tag{15}$$

where, u = x - y is the relative displacement between the lumped mass and base, F is the reaction force of the fluidic origami, ζ is the damping ratio, Ω is the excitation frequency, and Y is the base excitation amplitude. The reaction force (F) is determined based on the constitutive relationship of the fluidic origami (Equation (12)). In this section, we adopt a base-line ISMO design with a = b = 38 mm and $\gamma = 69^{\circ}$.

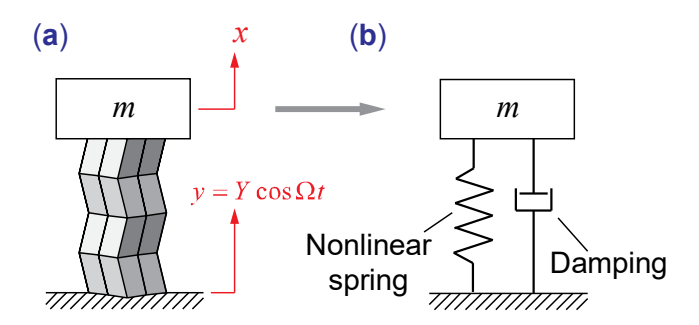


Figure 8. Setup for dynamic analysis. a) Schematic diagram of using fluidic origami for base vibration isolation. b) An equivalent system.

In order to harness the QZS property for low-frequency vibration isolation, the static equilibrium of the mass-spring-damper system shown in Figure 8 needs to occur at the QZS configuration. In other words, the weight of the lumped mass needs to equate the reaction force at the QZS point $(mg = F_{cr})$. To achieve this, one can exploit the unique property of pressurized fluidic origami mentioned in figure 5: that is, the magnitude of the reaction force at QZS configuration is linearly proportional to the magnitude of the initial pressure. Therefore, one can supply the initial pressure according to the following equation:

$$P_{i} = mg \left[-\left(\frac{V_{i}}{V}\right) \frac{dV}{dL} \right]^{-1} \bigg|_{QZS}$$
 (16)

To perform the dynamic analysis, the origin of reaction forcedeformation curve is moved to the QZS point on the curve (Figure 9). Near this point, a cubic polynomial fitting can be applied to approximate force-deformation relationship as follows:

$$F \approx \alpha x^3, \tag{17}$$

where the cubic stiffness coefficient α can be found via least square method. With the cubic stiffness approximation, the governing equation of motion (Equation (15)) is simplified to:

$$\ddot{u} + 2\zeta \dot{u} + \alpha u^3 = \Omega^2 Y \cos \Omega t, \tag{18}$$

which essentially represents a Duffing oscillator with a zero linear stiffness term. For the base line study and initial pressure of $P_i = 13.8 \text{ kPa}$, α turns out to be $81020 \, N/m^3$.

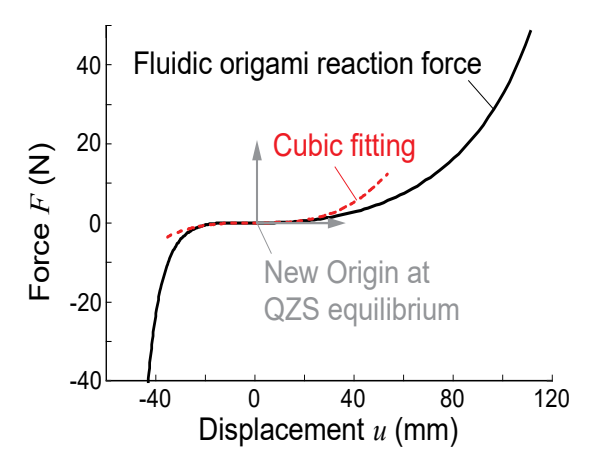


Figure 9. Applying cubic fitting to approximate the actual reaction force-deformation relationship of the fluidic origami

To measure the performance of the base excitation isolation, a transmissibility index (TR) is introduced as the ratio of the root mean squares of mass and base displacements, x and y, respectively:

$$TR = \frac{RMS(x(t))}{RMS(y(t))}. (19)$$

The actual governing equation of motion (Equation (15)), based on the actual force-displacement curve, is solved numerically using MATLAB "ode45" solver, and the steady-state time response solutions (shown in Figure 10) can be used to calculate the transmissibility index (TR). Beside numerical simulations, approximate solution based on the harmonic balance method (HBM) is also obtained in this research to provide a more efficient way to investigate the dynamic behavior of the fluidic origami with QZS property. HBM is a powerful

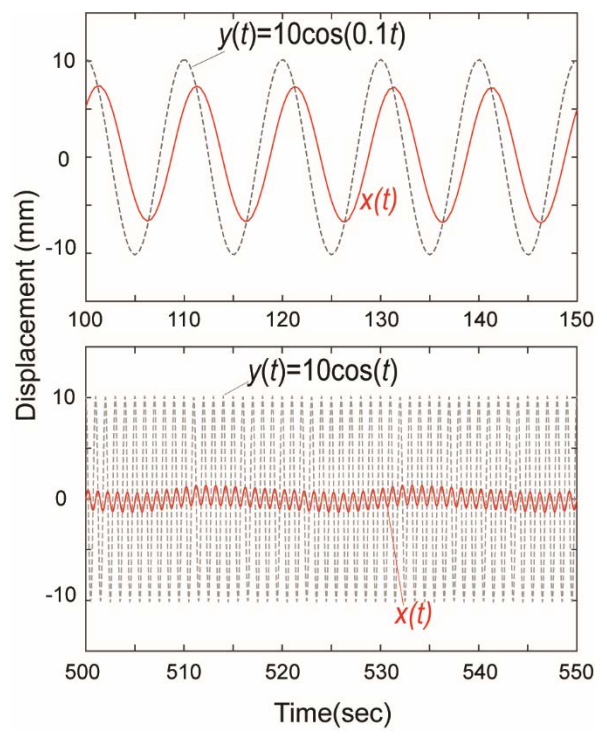


Figure 10. Sample time responses of base excitation isolation based on the actual force-displacement curve. (a) Ω =0.1 Hz and (b) Ω =1 Hz. The input amplitude of the base excitation is Y =10mm, and the initial condition of u(t) is [0,0].

method applicable to strongly nonlinear systems [33,35,36]. The solution of the equation of motion can be approximated as:

$$u = U_1 \cos \Omega t + U_2 \sin \Omega t. \tag{20}$$

Plugging this approximate solution into the dynamic equation (Equation (18)) and discarding higher order harmonic terms yield the following nonlinear polynomial equations:

$$\begin{cases} -\Omega^{2}U_{1} + 2\Omega\zeta U_{2} + \frac{3}{4}\alpha U_{1}^{3} + \frac{3}{4}\alpha U_{1}U_{2}^{2} - \Omega^{2}Y = 0\\ -\Omega^{2}U_{2} - 2\Omega\zeta U_{1} + \frac{3}{4}\alpha U_{2}^{3} + \frac{3}{4}\alpha U_{2}U_{1}^{2} = 0 \end{cases}$$
(21)

These two equations can be solved numerically to obtain the two unknown coefficients (U_1 , U_2), and transmissibility. Figure 11 shows the transmissibility index obtained by numerical simulation and HBM, which shows a good agreement.

Results of Figure 11 indicate that the pressure-induced quasizero stiffness from fluidic origami can indeed provide effective base excitation isolation at low frequency. The transmission index is consistently below 1 throughout the examined excitation frequency range (from 0 to 10Hz), indicating that the vibration

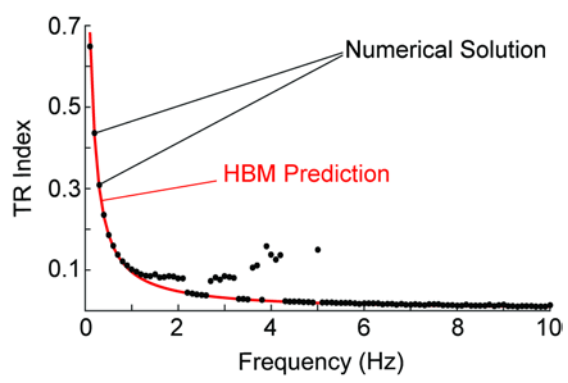


Figure 11. Transmission index of the fluidic origami. Solid line represents the results based on HBM, and solid dots represent simulation solution.

amplitude of the lumped-mass is always attenuated compared to the base. Furthermore, the static reaction force at QZS configuration (F_{cr}) is directly proportional to the initial pressure, which opens up the possibility to control fluidic origami on-demand according to any changes in the lumped mass. It can be seen that there exists some discrepancies between the numerical solution and the approximate HMB results for the medium frequencies. Further analysis shows that in that range of frequencies, dominant subharmonic oscillations have a significant role in the behavior of the system (figure 12). However, they have been neglected in the approximate solution based on the harmonic balance method. Nonetheless, such discrepancy does not negate the purpose using fluidic origami as vibration isolator because the transmissivity index remains well below one even with the discrepancy.

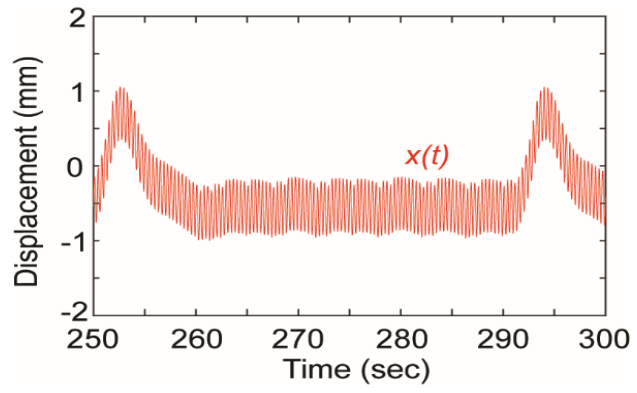


Figure 12. Time response of base excitation isolation based on the actual force-displacement curve for Ω =3 Hz. The input amplitude of the base excitation is Y =10mm, and the initial condition of u(t) is [0,0].

4. Conclusion

This research investigates the idea of harnessing the quasizero stiffness (QZS) property from the fluidic origami cellular solid for dynamic functionalities. Fluidic origami consists of

stacked Miura-Ori sheets, which have naturally embedded tubes that can be pressurized to induce unique stiffness properties. This research shows that if the pressurized air is sealed inside fluidic origami, the intricate and nonlinear relationship between folding and internal volume change can induce the quasi-zero stiffness. Two different design cases are studied to obtain the origami design guidelines for achieving QZS: One is identical stacked Miura-Ori sheets (ismo) and the other is non-identical stacked Miura-Ori. This study then turns its focus to the feasibility of harnessing the acquired quasi-zero stiffness for low-frequency base excitation isolation. Dynamic analyses based on approximate solutions (with harmonic balance method) are presented and compared to the numerical simulations. It is shown that QZS property from fluidic origami can provide effective base excitation isolation at low-frequencies. internal pressure of fluidic origami can also be adjusted to accommodate any changes in the system mass. results of this study can become the foundation of origamiinspired metamaterials and meta-structures with embedded dynamic functionalities.

5. Acknowledgement

The authors acknowledge the support from the National Science Foundation (award # CMMI-1633952) and the startup funding from Clemson University.

6. REFERENCES

- [1] McArthur, M., 2013, Folding Paper: The Infinite Possibilities of Origami, Tuttle Publishing, Rutland, VT, USA.
- [2] Schenk, M., Viquerat, A. D., Seffen, K. A., and Guest, S. D., 2014, "Review of Inflatable Booms for Deployable Space Structures: Packing and Rigidization," J. Spacecr. Rockets, 51(3), pp. 762–778.
- [3] Chen, Y., Peng, R., and You, Z., 2015, "Origami of Thick Panels," Science (80-.)., **349**(6246), pp. 396–400.
- [4] Filipov, E. T., Tachi, T., and Paulino, G. H., 2015, "Origami Tubes Assembled into Stiff, yet Reconfigurable Structures and Metamaterials," Proc. Natl. Acad. Sci., 112(40), pp. 12321–12326.
- [5] Felton, S., Tolley, M., Demaine, E. D., Rus, D., and Wood, R., 2014, "A Method for Building Self-Folding Machines," Science (80-.)., **345**(6197), pp. 644–646.
- [6] Randall, C. L., Gultepe, E., and Gracias, D. H., 2012, "Self-Folding Devices and Materials for Biomedical Applications," Trends Biotechnol., **30**(3), pp. 138–146.
- [7] Johnson, M., Chen, Y., Hovet, S., Xu, S., Wood, B., Ren, H., Tokuda, J., and Tse, Z. T. H., 2017, "Fabricating Biomedical Origami: A State-of-the-Art Review," Int. J. Comput. Assist. Radiol. Surg.

- [8] Ma, J., 2017, "A NOVEL ORIGAMI CRASH BOX WITH VARYING PROFILES," pp. 1–8.
- [9] Turner, N., Goodwine, B., and Sen, M., 2015, "A Review of Origami Applications in Mechanical Engineering," Proc. Inst. Mech. Eng. Part C J. Mech. Eng. Sci., **0**(0), p. 0954406215597713-.
- [10] Peraza-Hernandez, E. A., Hartl, D. J., Malak Jr, R. J., and Lagoudas, D. C., 2014, "Origami-Inspired Active Structures: A Synthesis and Review," Smart Mater. Struct., 23(9), p. 94001.
- [11] Lebée, A., 2015, "From Folds to Structures, a Review," Int. J. Sp. Struct., **30**(2), pp. 55–74.
- [12] Buchanan, M., 2017, "Physics under the Fold," Nat. Phys., **13**(4), pp. 318–318.
- [13] Schenk, M., and Guest, S. D., 2013, "Geometry of Miura-Folded Metamaterials," Proc. Natl. Acad. Sci., 110(9), pp. 3276–3281.
- [14] Eidini, M., and Paulino, G. H., 2015, "Unravelling Metamaterial Properties in Zigzag-Base Folded," (September), pp. 1–8.
- [15] Yasuda, H., and Yang, J., 2015, "Reentrant Origami-Based Metamaterials with Negative Poisson's Ratio and Bistability," Phys. Rev. Lett., **114**(18), p. 185502.
- [16] Fang, H., Li, S., Ji, H., and Wang, K. W., 2016, "Uncovering the Deformation Mechanisms of Origami Metamaterials by Introducing Generic Degree-Four Vertices," Phys. Rev. E, **94**(4), p. 43002.
- [17] Zhou, X., Zang, S., and You, Z., 2016, "Origami Mechanical Metamaterials Based on the Miura-Derivative Fold Patterns," Proc. R. Soc. A Math. Phys. Eng. Sci., 472(2191), p. 20160361.
- [18] Fang, H., Li, S., and Wang, K. W., 2016, "Self-Locking Degree-4 Vertex Origami Structures," Proc. R. Soc. A Math. Phys. Eng. Sci., 472(2195), p. 20160682.
- [19] Kamrava, S., Mousanezhad, D., Ebrahimi, H., Ghosh, R., and Vaziri, A., 2017, "Origami-Based Cellular Metamaterial with Auxetic, Bistable, and Self-Locking Properties," Sci. Rep., 7, p. 46046.
- [20] Hanna, B. H., Lund, J. M., Lang, R. J., Magleby, S. P., and Howell, L. L., 2014, "Waterbomb Base: A Symmetric Single-Vertex Bistable Origami Mechanism," Smart Mater. Struct., 23(9), p. 94009.
- [21] Waitukaitis, S., Menaut, R., Chen, B. G., and van Hecke, M., 2015, "Origami Multistability: From Single Vertices to Metasheets," Phys. Rev. Lett., **114**(5), p. 55503.
- [22] Daynes, S., Trask, R. S., and Weaver, P. M., 2014, "Bio-

- Inspired Structural Bistability Employing Elastomeric Origami for Morphing Applications," Smart Mater. Struct., **23**(12), p. 125011.
- [23] Silverberg, J. L., Na, J. H., Evans, A. A., Liu, B., Hull, T. C., Santangelo, C. D., Lang, R. J., Hayward, R. C., and Cohen, I., 2015, "Origami Structures with a Critical Transition to Bistability Arising from Hidden Degrees of Freedom," Nat. Mater., 14(4), pp. 389–393.
- [24] Li, S., and Wang, K. W., 2015, "Fluidic Origami with Embedded Pressure Dependent Multi-Stability: A Plant Inspired Innovation," J R Soc Interface, **12**(111), p. 20150639-.
- [25] Li, S., and Wang, K. W., 2015, "Fluidic Origami: A Plant-Inspired Adaptive Structure with Shape Morphing and Stiffness Tuning," Smart Mater. Struct., **24**(10), p. 105031.
- [26] Li, S., Fang, H., and Wang, K. W., 2016, "Recoverable and Programmable Collapse from Folding Pressurized Origami Cellular Solids," Phys. Rev. Lett., 117(11), p. 114301.
- [27] Yasuda, H., Chong, C., Charalampidis, E. G., Kevrekidis, P. G., and Yang, J., 2016, "Formation of Rarefaction Waves in Origami-Based Metamaterials," Phys. Rev. E, 93(4), p. 43004.
- [28] Ishida, S., Uchida, H., Shimosaka, H., and Hagiwara, I., 2015, "Design Concepts and Prototypes of Vibration Isolators Using Bi-Stable Foldable Structures," ASME International Design Engineering Technical Conferences and Computers and Information in Engineering Conference, ASME, Boston, MA, USA, p. V05BT08A030.
- [29] Fang, H., Li, S., Ji, H., and Wang, K. W., 2016, "Dynamics of a Bistable Miura-Origami Structure," Phys. Rev. E, p. In press.
- [30] Thomon, W. T., 2008, *Theory of Vibration with Applications*, Pearson.
- [31] Alabuzhev, P., Gritchin, A., Kim, L., Migirenko, G., Chon, V., Stepanov, P., and Rivin, E., 1989, Vibration Protecting and Measuring Systems with Quasi-Zero Stiffness, Hemisphere Publishing, NY.
- [32] Kovacic, I., Brennan, M. J., and Waters, T. P., 2008, "A Study of a Nonlinear Vibration Isolator with a Quasi-Zero Stiffness Characteristic," J. Sound Vib., **315**(3), pp. 700–711.
- [33] Carrella, A., Brennan, M. J., Kovacic, I., and Waters, T. P., 2009, "On the Force Transmissibility of a Vibration Isolator with Quasi-Zero-Stiffness," J. Sound Vib., 322(4–5), pp. 707–717.

- [34] Gramüller, B., Boblenz, J., and Hühne, C., 2014, "PACS—Realization of an Adaptive Concept Using Pressure Actuated Cellular Structures," Smart Mater. Struct., 23(11), p. 115006.
- [35] Nayfeh, A. H., 1993, Introduction to Perturbation Techniques, Wiley. New York.
- [36] Hamdan, M. N., and Burton, T. D., 1993, "On the Steady State Response and Stability of Non-Linear Oscillators Using Harmonic Balance," J. Sound Vib., **166**(2), pp. 255–266.